Article

Microfluidic Particle Engineering of Hydrophobic Drug with Eudragit E100—Bridging the Amorphous and Crystalline Gap

Swati Shikha, Yi Wei Lee, Patrick S. Doyle,* and Saif A. Khan*
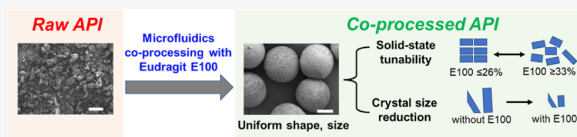
Read Online

ACCESS | Metrics & More | Article Recommendations | SI Supporting Information

ABSTRACT: Co-processing active pharmaceutical ingredients (APIs) with excipients is a promising particle engineering technique to improve the API physical properties, which can lead to more robust downstream drug product manufacturing and improved drug product attributes. Excipients provide control over critical API attributes like particle size and solid-state outcomes.

Eudragit E100 is a widely used polymeric excipient to modulate drug release. Being cationic, it is primarily employed as a precipitation inhibitor to stabilize amorphous solid dispersions. In this work, we demonstrate how co-processing of E100 with naproxen (NPX) (a model hydrophobic API) into monodisperse emulsions via droplet microfluidics followed by solidification via solvent evaporation allows the facile fabrication of compact, monodisperse, and spherical particles with an expanded range of solid-state outcomes spanning from amorphous to crystalline forms. Low E100 concentrations (≤26% w/w) yield crystalline microparticles with a stable NPX polymorph distributed uniformly across the matrix at a high drug loading (~89% w/w). Structurally, E100 incorporation reduces the size of primary particles comprising the co-processed microparticles in comparison to neat API microparticles made using the same technique and the as-received API powder. This reduction in primary particle size translates into an increased internal porosity of the co-processed microparticles, with specific surface area and pore volume ~9 times higher than the neat API microparticles. These E100-enabled structural modifications result in faster drug release in acidic media compared to neat API microparticles. Additionally, E100-NPX microparticles have a significantly improved flowability compared to neat API microparticles and as-received API powder. Overall, this study demonstrates a facile microfluidics-based co-processing method that broadly expands the range of solid-state outcomes obtainable with E100 as an excipient, with multiscale control over the key attributes and performance of hydrophobic API-laden microparticles.

KEYWORDS: particle engineering, droplet microfluidics, pharmaceutical crystallization, solid-state tunability, drug dissolution, powder rheology

1. INTRODUCTION

The transformation of small molecule active pharmaceutical ingredients (APIs) into high-quality solid oral dosage forms faces two major challenges. First, a vast majority of APIs exhibit poor powder flow properties that restrict their processability[1–4] and maximum loading in the final dosage form.[5–7] Second, a significant fraction of commercial APIs and those in discovery pipelines are hydrophobic, which limits their oral bioavailability in vivo.[8–10] Both powder flow and bioavailability of solid API are governed by the interplay of their critical quality attributes including particle morphology,[11–15] size,[10,16] and solid-state.[3,8,17–21] Co-processing APIs with excipients is a promising particle engineering technique to gain control over these critical attributes and manifest superior API performance.[22–26] Excipients, although non-therapeutic, play an indispensable role in oral dosage by serving as matrices to control drug loading,[27,28] solid-state outcomes,[28,29] and tune drug release.[15,28] With the APIs being exposed to varied pH conditions—highly acidic in the stomach (1–3) to physiological values (6–7.5) in the saliva and intestines—across the gastrointestinal tract, the use of pH-responsive excipients to modulate their release has gained significant traction in the last two decades.[30] Eudragit E100, belonging to a class of polymethacrylate-based copolymers, is one such widely used excipient with solubility in gastric fluid up to pH 5.[31–33] E100 is reportedly non-toxic[32] and is utilized for modulating drug release[34–39] and taste masking[31,37,38,40,41] in pharmaceutical formulations either on its own or in combination with other Eudragit[42,43] and non-Eudragit polymers.[36,44–46] The traditional utility of E100, however, has been heavily limited to generating amorphous solid dispersions by inhibiting precipitation of acidic[36,47–50] and basic APIs[51] via drug–excipient interactions. In this work, we demonstrate how co-processing of E100 with naproxen (NPX) (a model hydrophobic API) via a droplet microfluidics method allows the facile fabrication of

compact, monodisperse, and spherical particles with an expanded range of solid-state outcomes spanning from amorphous to crystalline forms.

APIs in amorphous state undergo a faster release due to their higher free energy,[8,17,52] but this poses phase transformation risks.[52,53] Additionally, amorphous solid dispersions largely show inferior flow properties.[19] Therefore, crystalline phases are generally preferred for long-term stability,[52−54] better control over the release,[21,54] and flow properties[3,18] by regulating the polymorphic form. In fact, a majority of the manufactured pharmaceutical APIs are delivered in the crystalline form.[55−58] Some prior studies[37,41,48,59] have reported crystalline outcomes for co-processed E100-API particles by increasing the API concentrations to overcome the interaction with E100. However, these studies do not demonstrate the necessary control over particle attributes critical for ensuring efficient release and robust manufacturability. For instance, a previous study optimized E100-artemether crystalline microparticle synthesis via a coacervation phase separation method with the primary objective to mask the bitterness of artemether.[37] The optimized formulation additionally had an improvement in drug release at an acidic pH but the polymorphic form, which influences powder flow, stability, and release, was not discussed. Moreover, the co-processing of E100 with API is generally performed via batch methods such as spray drying and bulk emulsification, which offer inadequate control over particle properties like morphology and drug loading.[40,48,60] In a previous study, E100-indinavir crystalline microparticles with different drug loads were generated via double emulsion−solvent evaporation method, but the microparticles obtained were polydisperse in size and irregularly shaped.[41] Non-uniform size distribution leads to inconsistencies in drug release[61] and results in poor powder flow due to mechanical interlocking.[14,16] Morphologically, a spherical shape has been shown to improve flow behavior,[11,12] as also demonstrated recently by our group.[13,14]

Here, we utilize a droplet microfluidics-based solvent evaporation technique to co-process E100 with NPX—a model hydrophobic, nonsteroidal anti-inflammatory drug—into spherical, monodisperse particles with control of solid-state phases, morphology, and internal structure, resulting in an improved drug release and flow behavior. Microfluidics-generated emulsions containing excipient and drug are obtained by dissolving both components in a common volatile solvent that is evaporated at room temperature to obtain solidified microparticles having shape, size, and drug distribution uniformity with high drug loadings. Notably, E100 incorporation enables both solid-state and structural control. By tuning the E100 concentrations, we observe solid-state tunability, with smaller E100 concentrations yielding stable crystalline forms. Further characterizations of the crystalline microparticles of E100-NPX reveal modifications of the inner porosity of microparticles and the sizes of primary particles comprising them, when compared to the NPX microparticles prepared similarly, albeit without the excipient. Crucially, these modifications contribute to a faster drug release from the co-processed E100-NPX microparticles in the acidic release media with NPX present in the crystalline form. The fine control over particle attributes by careful combination of excipient and microfluidics-based particle engineering results in improved powder flow properties compared to neat NPX microparticles and raw NPX. Overall, this study expands the utility of E100 beyond its conventional use as a precipitation inhibitor and demonstrates the synthesis of stable crystalline microparticles of a hydrophobic API with finely tuned particle attributes via a simple, yet efficient particle engineering technique, thus broadening its utility for developing "designer" pharmaceutical formulations.

2. EXPERIMENTAL SECTION

2.1. Materials. NPX (N8280), polyvinyl alcohol (PVA, Mowiol 8-88, MW ∼ 67,000 g mol⁻¹), dichloromethane (DCM anhydrous, ≥99.8%, contains 40−150 ppm amylene as stabilizer), sodium chloride (NaCl, ACS reagent, ≥99.0%), and hydrochloric acid (HCl, 37%, ACS reagent) were purchased from Sigma-Aldrich and used as received. Eudragit E100 was procured as a gift from Evonik. Ultrapure water (18.3 MΩ) was used from a Sartorius Arium pro ultrapure water purifier. Fluorinated ethylene propylene (FEP) tubing (0.032″ inner diameter) for outlet, polytetrafluoroethylene (PTFE) tubing (0.33 mm inner diameter) to dispense the dispersed and continuous phase, and MicroCross poly(ether ether ketone) (PEEK) cross-junction (0.006 in. thru hole) were purchased from Scientific Commodities Inc., GL Sciences, and IDEX Health & Science LLC, respectively. Phosphate-buffered saline (PBS, ultrapure grade) with pH 7.4 ± 0.2 was bought from Vivantis and diluted to a 1× solution with ultrapure water for further use.

2.2. Eudragit E100-NPX Microparticle Synthesis. Eudragit E100 and NPX were co-dissolved in DCM at different concentration ratios of 0.125:1, 0.25:1, 0.35:1, 0.5:1, and 1:1, which correspond to 6.25, 12.5, 17.5, 25, and 50 mg/mL of E100, respectively, with NPX at 50 mg/mL to form the dispersed phase, which was filtered through 0.45 μm PTFE filters prior to use. The first numbers in the ratio are used to refer to the E100-NPX formulations henceforth. The aqueous continuous phase was prepared by dissolving 1.5 wt % PVA as a surfactant to stabilize the oil-in-water emulsions in ultrapure water and filtered using a 0.2 μm nylon filter. The dispersed phase and continuous phase were infused into a 1/16″ PEEK cross-junction (0.006 in. thru-hole) using Harvard apparatus syringe pumps (Harvard PHD ULTRA 70-3007) at 40 and 200 μL/min flow rates, respectively. The emulsions generated were collected via an FEP outlet tube in a 50 mm Petri dish with 1.5 wt % aqueous PVA solution and subjected to shaking on an orbital shaker (BOECO OS-20) at 100 rpm for solidification via evaporative crystallization at room temperature. Solidified E100-NPX microparticles were washed with ultrapure water using a cell strainer (pluriSelect) of 150 μm mesh size and dried at room temperature (∼22 °C) under vacuum overnight before further use. Neat NPX (50 mg/mL) and neat E100 (50 mg/mL) microparticles were also prepared as controls in the same manner outlined above.

Thermogravimetric analysis (TGA, Shimadzu) was used to quantify residual moisture in the co-processed microparticles. For this, around 5 mg of E100-NPX 0.25 microparticles was weighed in an alumina pan followed by a scan from 30 to 600 °C at a heating rate of 10 °C min⁻¹. Mass loss was recorded as a function of change in temperature. A benchtop Spinsolve ULTRA nuclear magnetic resonance (NMR) from Magritek operating at 60 MHz was used to quantify the residual DCM in the vacuum-dried microparticles. For this, around 10 mg of E100-NPX 0.25 microparticles was added to 750 μL of deuterated chloroform (CDCl₃) with 14 μL of mesitylene (1,3,5-trimethylbenzene) used as an internal reference.

2.3. Solid-State Outcomes and Drug−Excipient Interactions. *2.3.1. Solid-State and Polymorph Characterization.* The solid-state and polymorphic outcomes of NPX in different formulations of E100-NPX microparticles and neat microparticles were analyzed via powder X-ray diffraction (PXRD) and differential scanning calorimetry (DSC) analysis. An X-ray diffractometer (Bruker, D8 ADVANCE) with Cu radiation at a wavelength of 1.54 Å operating at 40 kV, 30 mA, and at a scanning rate of 0.78°/min over a 5−40° range of 2θ was used. DSC thermograms were acquired in a heat−cool−heat manner using a DSC25 apparatus (TA instruments) where around 5 mg of particles was sealed in an aluminum pan with a pinhole and heated from −10 to 200 °C/min at 10 °C/min in the first heat scan. Next, the samples were equilibrated (at ∼50 °C/min) to −10 °C to delete the existing thermal history followed by a second heat scan from −10 to 200 °C with a 10 °C/min ramp rate. An empty crimped pan with a pinhole was used as the reference. Dry nitrogen at a flow rate of 50 mL/min was used as the purge gas.

2.3.2. Drug−Excipient Interactions. The drug−excipient interaction was assessed using the attenuated total reflection (ATR) method by VERTEX 70 Fourier transform infrared (FTIR) spectroscopy (Bruker). Neat NPX, neat E100, and E100-NPX microparticles were placed on the sample stage, and spectra were recorded from 4000 to 500 cm^{-1} with 32 scans averaged at a resolution of 4 cm^{-1}.

2.4. Macro and Microscale Characterization of Co-Processed Microparticles. *2.4.1. Uniformity of Size, Shape, and Loading Characterization.* A field emission scanning electron microscope (FESEM, JEOL JSM-7610F Plus) operating at 5 kV accelerating voltage was used to characterize the morphology of raw NPX and microfluidics-generated neat NPX and E100-NPX microparticles. Samples were prepared on the conventional scanning electron microscopy stubs with the carbon tape, and some of them were manually cross-sectioned followed by sputter-coating with ∼10 nm of platinum.

Bright-field microscopy (Olympus CKX41 coupled with Olympus cellSens entry imaging system) images were acquired to measure the size and size distribution of raw NPX, neat NPX microparticles, and E100-NPX microparticles with and without E100. Sizes of more than 100 microparticles were calculated via ImageJ and plotted as a histogram. The polydispersity index (PDI) was calculated as the square of the ratio of standard deviation to the mean. The particle sizes of raw NPX (as-received from Sigma) were determined using the "regionprops" function of MATLAB (MathWorks) after Otsu thresholding to obtain particle area, major (crystal length), and minor axis (crystal width). The area of each particle was transformed to the area-equivalent diameter and plotted as a histogram.

To gauge the sizes of primary particles comprising the microparticles, neat NPX and E100-NPX 0.25 microparticles were disintegrated by sonicating (Elmasonic S 60 H) them for 1 min in ultrapure water at 1 mg/mL. A small amount of solution with dispersed primary crystals was carefully pipetted out and imaged using a glass flow cell (channel dimensions: 200 μm deep, 3 cm long, 1 mm wide) immediately using a bright-field microscope to avoid changes in initial crystal size due to agglomeration or Ostwald ripening. The acquired images were analyzed for the size and size distribution of primary particles following the same method as described above for raw NPX particles.

Drug distribution uniformity within a particle was analyzed by Raman mapping (Renishaw inVia confocal Raman spectrom-

eter) for E100-NPX 0.25 microparticles. The spectra were recorded with a 532 nm laser excitation using 1200 g/mm grating at 50× magnification with 10 s acquisition time and two accumulations. Raman point-by-point mapping sized 220 × 220 μm was performed in both x and y directions for the surface and at a confocal depth of ∼100 μm with a resolution of 2 μm per point. Data processing was carried out using the in-built windows-based Raman Environment (WiRE) software version 5.2.

2.4.2. Specific Surface Area and Pore Volume. The specific surface area and pore volume were measured for microparticles with and without excipient using a Micromeritics 3Flex instrument with nitrogen at −196 °C after degassing the samples for 16 h at room temperature. Data processing was performed using the in-built 3Flex software version 5.02. Brunauer−Emmett−Teller (BET) specific surface area was deduced from the adsorption isotherm using the multipoint technique in the relative pressure range of 0.05−0.3, and total pore volume was obtained from single-point desorption at a relative pressure of 0.95.

2.5. Drug Loading and In Vitro Drug Release. *2.5.1. Drug Loading.* Drug loading was performed in triplicates by sonicating 2−3 mg of co-processed E100-NPX microparticles in 2 mL of isopropyl alcohol (IPA, ≥99.7%, AnalaR NORMAPUR ACS, VWR) for 30 min. The solution was filtered by a 0.22 μm PTFE filter and diluted with IPA before measuring the drug concentration using the Cary 60 UV−visible spectrophotometer. For quantification, a calibration curve was prepared with the known concentrations of NPX in IPA at a 272 nm wavelength.

2.5.2. Drug Release. In vitro drug release was performed in triplicates for neat NPX microparticles and E100-NPX 0.125, 0.25, and 0.35 crystalline microparticles in release media with pH 7.4 and 1.2. For pH 7.4, 10× PBS from Vivantis was diluted to 1× using ultrapure water. Microparticles with and without excipient were added to 80 mL of 1× PBS and stirred on an orbital shaker (PSU-10i, Biosan) at 200 rpm at 37 °C. The mass of neat NPX and E100-NPX microparticles with different concentrations of E100 was added such that the final NPX concentration in the release media was ∼40 μg/mL.

For pH 1.2, simulated gastric fluid (SGF) without enzyme was prepared by dissolving 2 g of NaCl in 900 mL of ultrapure water.[62,63] The pH was adjusted to 1.2 using 37% HCl, and the final volume was made up to 1000 mL. Before conducting the release study, the solubility of NPX at pH 1.2 was evaluated. The as-received raw NPX (∼10 mg) was added to 10 mL of SGF and magnetically stirred at 1000 rpm for 2 days at 37 °C followed by 2 days of standing to achieve equilibrium. The solution was filtered through a 0.45 μm nylon filter, and UV−visible spectra were recorded at 272 nm. NPX solubility in SGF at 37 °C was quantified based on the calibration curve of NPX in SGF at 272 nm. For the release study, the mass of neat NPX and E100-NPX microparticles was added such that the final NPX concentration in SGF was ∼6 μg/mL. The higher volume of SGF (pH 1.2) release media compared to PBS (pH 7.4) is due to the poor solubility of NPX in acidic media. Stirring speed and temperature were maintained at 200 rpm and 37 °C, respectively. For all the release studies, 1 mL of release media was carefully pipetted out at predetermined time intervals to measure the apparent free drug using a Cary 60 UV−visible spectrophotometer, and 1 mL of fresh media was added to maintain the sink conditions. Cumulative drug release

percentage was quantified based on the calibration curve of NPX in the respective release medium at 272 nm.

2.6. Powder Flow Characterization. Powder flow behavior was compared for unprocessed raw NPX and microfluidics-generated neat NPX and E100-NPX 0.25 microparticles. The three different powder types were subjected to a shear cell test using an FT4 rheometer from Freeman Technology. Powders were added in a 1 mL shear cell module and conditioned before applying pre-consolidation normal stress of 3 kPa with a 24 mm flat-surface vented piston. Incipient shear stresses for yielding were obtained as a function of normal stresses of 1, 1.25, 1.5, 1.75, and 2 kPa using a 24 mm bladed shear head. The incipient failure points and pre-shear points were plotted against their corresponding normal stress, and a yield locus was obtained using the inbuilt FT4 analysis software. Measurements for each powder sample were performed in triplicates, and shear stress data were fitted using OriginPro 2019.

3. RESULTS AND DISCUSSION

3.1. Co-Processing of E100-NPX Microparticles Using Droplet Microfluidics. Eudragit E100 is composed of dimethylaminoethyl methacrylate, butyl methacrylate, and methyl methacrylate at a molar ratio of 2:1:1 with cationic property at lower pH values, owing to the presence of tertiary amine groups (Figure 1a).[32,33,64,65] On the other hand, NPX is a
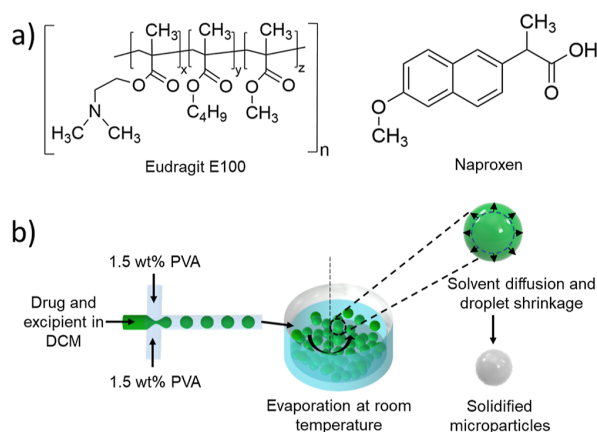

Figure 1. (a) Chemical structures of Eudragit E100 terpolymer (x: dimethylaminoethyl methacrylate, y: butyl methacrylate, and z: methyl methacrylate at a molar ratio of 2:1:1 distributed randomly along the copolymer chain) and NPX (b) scheme outlining the steps of co-processing E100 with NPX using droplet microfluidics.

hydrophobic BCS class II API,[66] that exists in the anionic form at higher pH values due to the deprotonation of carboxyl groups (Figure 1a).[29,64] E100 and NPX were co-dissolved in DCM as the dispersed phase and confined into droplets using 1.5 wt % aqueous PVA as the continuous phase, as shown schematically in Figure 1b. The droplets were routed for collection as a monolayer in a Petri dish filled with a 5 mm film of 1.5 wt % aqueous PVA. After collection, the Petri dish was transferred to an orbital shaker operating at 100 rpm at room temperature. During shaking, DCM evaporates from the droplets due to its high volatility, owing to high vapor pressure leading to supersaturation and subsequent solidification via polymer vitrification and/or drug crystallization marked by the trans-

formation of translucent droplets into opaque white solids. The ensemble of droplets did not coalesce during collection and shaking.

The solidified microparticles were washed using ultrapure water and vacuum dried before further use. Using this protocol, a range of E100-NPX microparticles with varying E100 to NPX concentration ratios—0.125, 0.25, 0.35, 0.5, and 1 along with neat NPX and neat E100 microparticles were prepared. Residual moisture in the dried E100-NPX 0.25 microparticles was found to be 2.5% (w/w) using TGA (Figure S1a, Supporting Information). Residual DCM in the dried E100-NPX 0.25 microparticles was quantified to be 0.04 wt % using proton NMR (Figure S1b,c, Supporting Information). Considering the median average daily dose of NPX as 1000 mg/day,[67] the residual DCM amount in the microparticles corresponded to 0.4 mg/day, which is 15 times lower than the ICH's permissible daily exposure limit of 6 mg/day for DCM.[68]

3.2. Tunability of Solid-State Outcomes. Obtaining the correct solid-state outcome is essential for the successful manufacturing of the drug product in the required dosage form with desired therapeutic efficacy. Solid-state outcomes were evaluated using PXRD and DSC. PXRD spectra showed crystalline peaks for neat NPX and E100-NPX 0.125, 0.25, and 0.35 microparticles (Figure 2a) that consistently correspond to NPX form I, with characteristic peaks at 6.6, 12.7, 19, 20.4, 22.6, 23.7, 27.4, 27.8, and 28.6°, which is reportedly one of the most stable and preferred forms of NPX.[66] For neat E100 and E100-NPX 0.5 and 1 microparticles, no such peaks were observed, indicating an amorphous state of NPX.

Thermal analysis performed using DSC in a heat-cool-heat manner further ascertained the solid-state outcomes. The DSC data for melting temperatures from the first and second heat scans and glass-transition temperatures (T_{gs}) from the second heat scans are compiled in Table 1. Neat NPX microparticles had a sharp melting peak at 157 °C in the first heat scan (Figure 2c), which is close to the previously reported melting point for form I of NPX.[66] The drug then recrystallizes from the melt during the cooling cycle marked by the appearance of an upward exothermic peak (data not shown), owing to its high crystallization ability followed by a downward endothermic melting peak again at 157 °C in the second heat cycle (Figure 2d).[64,69,70] With the addition of E100, formulations with smaller E100 concentrations, E100-NPX 0.125, 0.25, and 0.35, showed melting peaks attesting the crystallinity of NPX. However, the endotherms were relatively broader with reduced melting points at 155, 149, and 140 °C observed for E100-NPX 0.125, 0.25, and 0.35, respectively. While drug recrystallization from the melts for E100-NPX 0.125 and 0.25 microparticles occurred in the second heat scan instead of the cooling cycle, no recrystallization event was observed for E100-NPX 0.35 microparticles. In contrast, no melting peak was recorded for formulations with higher E100 concentrations (E100-NPX 0.5 and 1), indicating the trans-formation of NPX to an amorphous state. These changes in the solid-state, melting profiles, and recrystallization ability of NPX in the presence of E100 suggested high miscibility of drug and polymer likely due to their intermolecular interactions.[27,28,36,40,48,70,71] Additionally, the glass-transition temperatures (T_{gs}) obtained from the second heat scans revealed a reduction for all the E100-NPX microparticles compared to that of neat E100 particles (T_g, 47 °C) likely due to NPX acting as a plasticizer. These experimentally obtained T_{gs} from the second heat scan of DSC were found to be higher than the T_g values predicted by the Gordon−Taylor equation further emphasizing
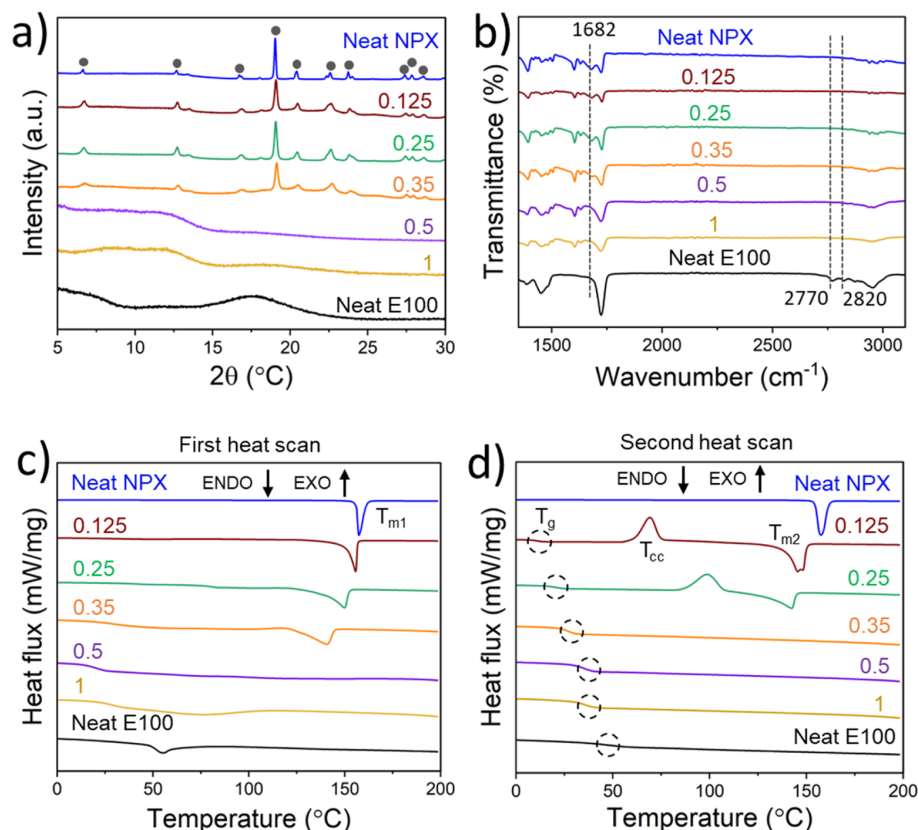
Figure 2. Solid-state outcomes and drug−polymer interactions for neat NPX, E100-NPX 0.125, 0.25, 0.35, 0.5, and 1 and neat E100 microparticles (top to bottom) via (a) PXRD spectra show crystallinity of NPX in neat NPX and E100-NPX 0.125, 0.25, and 0.35 microparticles with characteristic peaks marked in black circles corresponding to form I of NPX. (b) ATR−FTIR spectra with peaks at 2770 and 2820 cm^{-1} representing non-protonated dimethylamine groups of pure Eudragit E100, and the peak at 1682 cm^{-1}, representing hydrogen-bonded carbonyl groups. DSC thermograms of (c) first and (d) second heat scans, where T_{m_1} and T_{m_2} are melting temperatures (downward peaks) from the first and second heat scans, T_g (circles) is glass-transition temperature from the second heat scan, and T_{cc} is the cold-crystallization temperature (upward peaks) from cooling (neat NPX) or second heat scan (E100-NPX 0.125 and 0.25). The melting point of NPX at 157 °C corresponds to form I of NPX.

Table 1. Summary of Thermal Events (Melting Temperatures from First (T_{m_1}) and Second (T_{m_2}) Scans, Normalized Melting Enthalpy from First Heat Scan (H_{mI}), Glass-Transition Temperature (T_g) from Second Heat Scan, and Cold Crystallization Temperature (T_{cc}) from DSC Heat-Cool-Heat Scan for Different E100-NPX Formulations

formulations	E100 (mg/mL)	NPX (mg/mL)	T_{m_1} (°C)	H_{m_1} (J/g)	T_g (°C)	T_{cc} (°C)	T_{m_2} (°C)	% crystallinity
neat NPX (100% NPX)	0	50	157.3	140		96.5 (cooling)	157.4	100
E100-NPX 0.125 (11% E100−89% NPX)	6.25	50	155.5	77.5	10.9	69.5(second heat)	145.2	62
E100-NPX 0.25 (20% E100−80% NPX)	12.5	50	149.3	39.6	20.5	101.1(second heat)	141.9	35
E100-NPX 0.35 (26% E100−74% NPX)	17.5	50	140.4	20.8	26.6			20
E100-NPX 0.5 (33% E100−67% NPX)	25	50			34.87			
E100-NPX 1 (50% E100−50% NPX)	50	50			34.55			
neat E100 (100% E100)	50	0			47.45			

the drug−excipient interactions (see Section S2, Supporting Information for details). Appearance of single T_{gs} for all the E100-NPX formulations and their positive deviations from the predicted T_{gs} (from Gordon−Taylor equation) suggest drug-excipient miscibility with no phase separation, as also reported in previous studies.[40,50,64,72] However, smaller domains (less than 30 nm) with more than one phase are difficult to detect using DSC, necessitating the use of other techniques to ascertain the existence of a single phase.[64,73−75]

Based on the normalized melting enthalpies of the first heat scan of DSC endotherms, percent crystallinity was calculated for E100-NPX 0.125, 0.25, and 0.35 microparticles as reported earlier[76]

$$\% \text{ crystallinity} = \frac{\Delta H_{m_1}}{\Delta H_{m_1(100\%)} \times w} \times 100 \tag{1}$$

where ΔH_{m_1} and $\Delta H_{m_1(100\%)}$ are the normalized melting enthalpies (J/g, normalized to total sample mass) of the co-
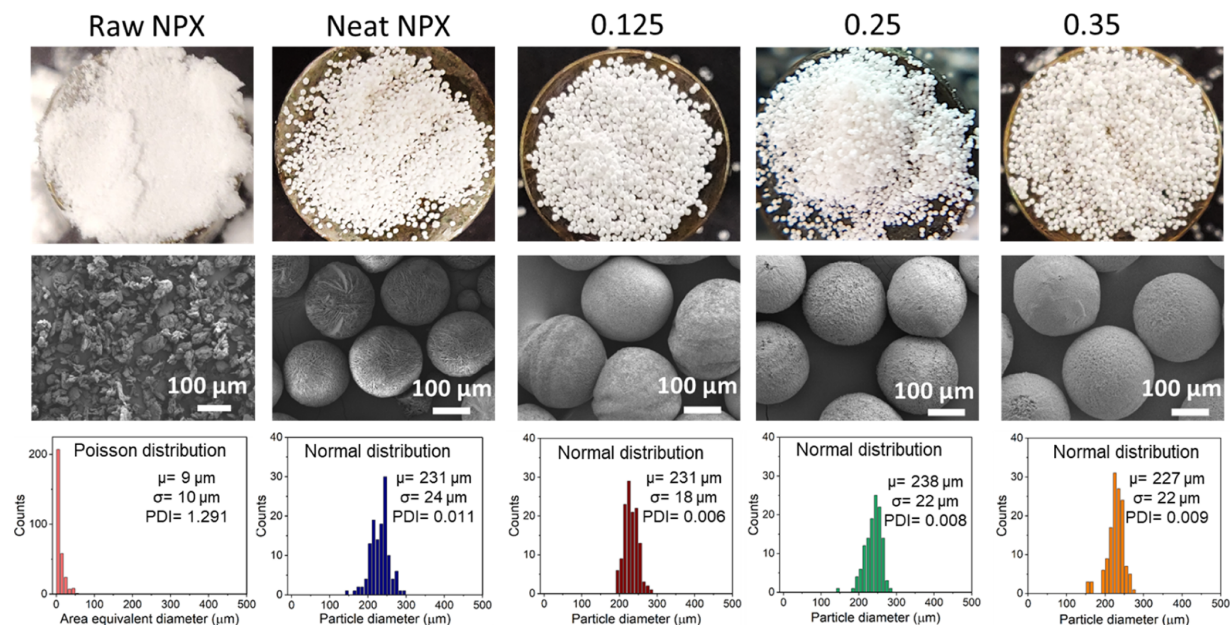
Figure 3. Macroscale camera images (top panel), FESEM images (middle panel), and particle size distributions (bottom panel) of raw NPX, neat NPX, E100-NPX 0.125, E100-NPX 0.25, and E100-NPX 0.35 microparticles (from left to right).

processed E100-NPX microparticles and neat NPX (100% crystalline) microparticles from the DSC thermograms of first heat scans, respectively, and w is the actual weight fraction of NPX in the co-processed microparticles. For neat NPX microparticles, the normalized melting enthalpy was found to be 140 J/g which was the same as that observed for raw NPX (as received from Sigma). Hence, the value of melting enthalpy for neat NPX microparticles was chosen as the reference for 100% crystalline material. The normalized melting enthalpies for E100-NPX 0.125, 0.25, and 0.35 obtained from the first heat scans were found to be 77.5, 39.6, and 21 J/g, respectively (Table 1). Based on the actual NPX weight fraction in these co-processed microparticles, the degree of crystallinity was found to be 62, 35, and 20%, respectively. The remaining amount of NPX in the co-processed microparticles is present in the amorphous form and stabilized by E100 via drug−excipient interactions.

To confirm the E100-NPX interaction, ATR−FTIR spectroscopy measurements were performed for neat microparticles and E100-NPX microparticles (Figure 2b). For neat E100 microparticles, peaks appearing at 2770 and 2820 cm^{-1} were assigned to the non-protonated dimethylamine groups and were found to disappear with the addition of NPX signifying their protonation. Markedly, the peak at 1682 cm^{-1} assigned to the hydrogen-bonded carbonyl groups in neat NPX microparticles was observed to be reducing in intensity for E100-NPX 0.125, 0.25, and 0.35 microparticles, indicating their deprotonation to participate in the ionic interaction with the protonated tertiary amines of E100. With further increase in E100 concentrations for E100-NPX 0.5 and 1 microparticles, the peak at 1682 cm^{-1} disappeared entirely, due to the extensive interaction between E100 and NPX leading to complete amorphization of NPX in these formulations. These findings are in accordance with the solid-state outcomes observed via PXRD and DSC data and previously reported studies on the interaction of Eudragit E100 with NPX and other anionic APIs.[29,60,64,77−80] There is also a possibility of ester groups of E100 being involved in the ionic

interaction, as reported earlier by Ueda et al.[64] However, this could not be established due to the presence of an overlapping peak of free carbonyl groups of NPX at 1725 cm^{-1}. After screening the solid-state outcomes, further characterizations of attributes and performances were conducted for crystalline E100-NPX microparticles.

3.3. Structure, Size, and Drug Distribution Uniformity for Crystalline Microparticles. Shape, size distribution, and drug distribution uniformity are highly desired to ensure consistency of release and powder flowability of the drug particles.[27,81] Batch methods to co-process APIs with E100 excipient offer coarse control over particle morphology, yielding irregularly shaped agglomerates with broad size distributions and non-uniform loading of hydrophobic APIs.[41] Visually, our droplet microfluidics-based particle engineering method yielded microparticles that are distinct spheres, compared to the fine raw NPX powder (Figure 3, top panel). Under FESEM imaging, the microfluidics-processed neat NPX microparticles and E100-NPX crystalline microparticles appeared uniformly spherical, while raw NPX particles were irregularly shaped with plate-like morphology (Figure 3, middle panel). The particle size distribution for all the samples was analyzed using bright-field microscopy imaging (Figure S3, Section S3, Supporting Information) and plotted as histograms (Figure 3, bottom panel). Raw NPX powder had the smallest particle size (9 ± 10 μm) and highest PDI (1.291) following a Poisson distribution. In contrast, all the microfluidics-generated particles displayed a normal size distribution with similar average particle sizes ranging from ∼230 to 240 μm with significantly reduced PDI values of 0.011, 0.006, 0.008, and 0.009 for neat NPX and E100-NPX 0.125, 0.25, and 0.35 microparticles, respectively. The size and shape uniformity of the processed microparticles is attributed to the monodispersity of the emulsions generated using droplet microfluidics.

To ascertain the drug loading uniformity within a particle, spatial drug distribution was evaluated using confocal Raman
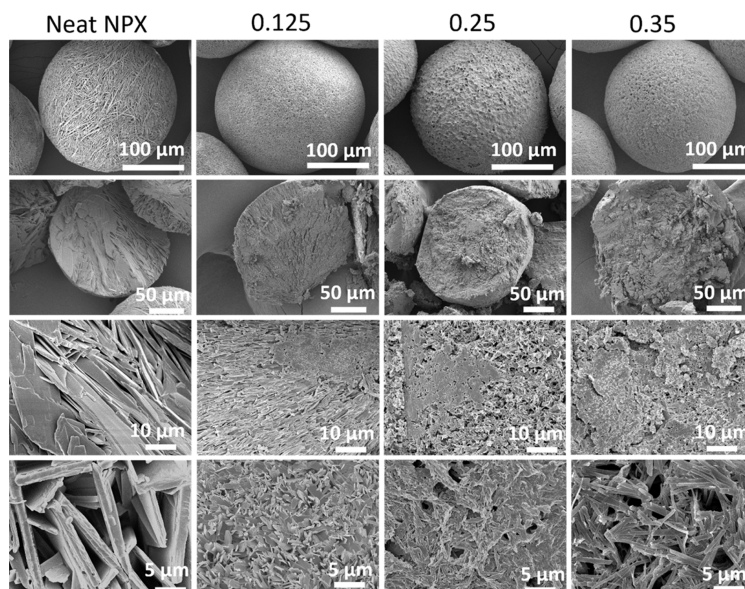
Figure 4. FESEM images of primary particles on the particle surface and in the cross-sections shown at various magnifications for neat NPX, E100-NPX 0.125, E100-NPX 0.25, and E100-NPX 0.35 microparticles, in columns from left to right.

mapping for E100-NPX 0.25 microparticles as a proof-of-concept. First, Raman spectra for neat microparticles were recorded using a 532 nm excitation laser, and Raman shifts at 600 and 742 cm^{-1} were identified specific to E100[82] and NPX,[83] respectively (Figure S4a, Section S3, Supporting Information). These peaks were found to be present both at the surface and the confocal depth of ∼100 μm for E100-NPX 0.25 microparticles. The peak for E100 was weaker likely due to its small amount (20%) in E100-NPX 0.25 microparticles compared to that of neat E100 microparticles. Mapping was then performed in a point-by-point manner, and x−y maps were constructed using the intensity ratio of drug to polymer that highlighted uniform drug distribution both at the surface and the confocal depth of ∼100 μm for E100-NPX 0.25 microparticles (Figure S4b, Section S3, Supporting Information).

3.4. Probing Particle Microstructure. In addition to the overall particle properties, attributes at the sub-particle level influence the powder rheology and drug release.[1] When crystallized in the presence of foreign substances like excipients, the nucleation kinetics of an API often get modulated, leading to changes in their final crystal size.[84] Additionally, particle engineering methods using solvent removal through the polymeric matrix have been shown to create porous internal structures.[15,27,85] For overcoming the poor solubility of hydrophobic APIs, a porous matrix is highly preferred as it facilitates faster ingression of release media.[1,86−88] Having a smaller size of the primary particles is desirable to further accelerate the release through more surface area in contact with the release media.[10] On the other hand, differences in crystal habits influence the contact area and friction between the particles which affects flowability.[14,89] Therefore, we investigated the primary particles and porosity of microfluidics-generated microparticles with and without E100.

FESEM images at higher magnifications highlighted bigger, lath-like primary particles on the surface as well as in the cross-sections of the neat NPX microparticles (Figure 4). In comparison, E100-NPX 0.125, 0.25, and 0.35 microparticles

comprised of primary particles with smaller sizes. Furthermore, primary particles obtained post-sonication for neat NPX microparticles had a larger area equivalent diameter (6 ± 5 μm) and aspect ratio (4 ± 5) compared to those for E100-NPX 0.25 microparticles (area equivalent diameter, 2 ± 1 μm; aspect ratio, 1.6 ± 0.5) (Figure S5, Section S4, Supporting Information). This reduction in the size of the primary particles for E100-NPX microparticles could be attributed to the presence of E100, which likely enhances the nucleation rate by reducing the nucleation free-energy barrier, thereby yielding smaller-sized crystals.[84]

BET analysis further showed that E100 incorporation increased the overall internal porosity with E100-NPX 0.25 microparticles having both specific surface area (6.61 m^2/g) and pore volume (8.93 × 10^{-3} cm^3/g) ∼9 times higher compared to the neat NPX microparticles (specific surface area, 0.77 m^2/g and pore volume, 0.96 × 10^{-3} cm^3/g) (Figure S6, Section S4, Supporting Information).

3.5. Performance Characterization: Drug Loading, In Vitro Release, and Powder Flow. After characterizing the polymorphic and structural attributes of the API in the microparticles at the particle and primary particle levels, we studied the performance of the co-processed E100-NPX microparticles in terms of the drug loading, in vitro release, and powder flow.

3.5.1. Drug Loading. Drug loading and entrapment efficiency were analyzed for E100-NPX 0.125, 0.25, and 0.35 micro-particles using eqs 2 and 3, based on the NPX calibration curve in IPA at 272 nm. Notably, E100 did not interfere with the drug measurement at the specified wavelength.[90]

$$\% \text{ drug loading} = \frac{\text{mass of drug in particles}}{\text{total mass of particles}} \times 100 \tag{2}$$

$$\% \text{ entrapment efficiency} = \frac{\text{mass of drug in particles}}{\text{initial mass of drug added}} \times 100 \tag{3}$$

Experimental drug loading across the triplicates was calculated to be ~89, 80, and 74% for E100-NPX 0.125, 0.25, and 0.35, respectively, which is similar to their theoretical loading (Table S1, Section S5, Supporting Information). Based on the initial mass of the NPX used, the entrapment efficiency was calculated to be ~100%. The poor NPX solubility in aqueous 1.5 wt % PVA, used to generate and collect the emulsions, likely prevents API loss during DCM diffusion, thereby leading to efficient drug loadings in E100-NPX microparticles prepared via microfluidics-based evaporative solidification.

3.5.2. In Vitro Drug Release. Drug release studies were conducted to evaluate the impact of E100 excipient on the release of NPX, as compared to neat NPX microparticles at pH 1.2 (SGF) and pH 7.4 (PBS) resembling gastric and neutral pH, respectively (Figure 5). The percentage of NPX released was
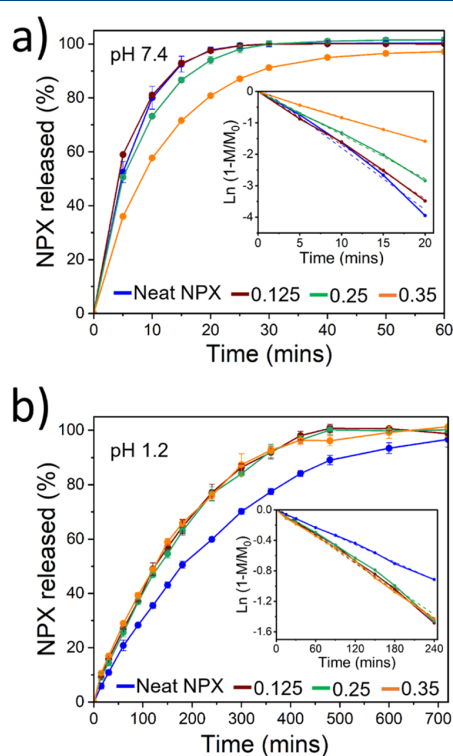

Figure 5. In vitro drug release profiles for neat NPX (blue curves) and E100-NPX 0.125 (brown curves), 0.25 (green curves), and 0.35 (orange curves) microparticles at (a) pH 7.4 and (b) pH 1.2 with the insets showing their first-order release kinetics. The curves in the release profiles do not represent the first-order fits and are drawn to serve as a visual guide to the eyes. Error bars correspond to standard deviations for triplicates for each group. M_0 is the initial mass of NPX in the microparticles, and M is the released mass at different time points.

calculated by the cumulative drug mass released normalized with the actual drug mass present in the weighed neat NPX and E100-NPX microparticles. Dissolution kinetics extracted from the plot of the logarithm of cumulative drug remaining percent as a function of time are plotted as insets in Figure 5, and the values are summarized in Table S2, Supporting Information.

At pH 7.4, neat NPX microparticles showed fastest release (Figure 5a) with complete dissolution by 30 min, owing to the high solubility (~1 mg/mL) of NPX at this pH.[91] E100-NPX

0.125 microparticles had a similar release profile as that of neat NPX microparticles, likely because of the small amount of E100 (11%) and the smaller sizes of primary particles. Further increase in the excipient amount of the microparticles led to a reduction in drug release rates, with E100-NPX 0.35 (26% E100) microparticles showing the slowest release which was completed after 1 h. This delay in release with increasing excipient concentration is due to the insolubility of E100 polymer at pH > 5.[37] The undissolved remnants of E100-NPX microparticles after 2 h of release were retrieved by filtration through a 40 μm strainer, washed thrice with ultrapure water to remove the release media, and vacuum dried prior to characterization for the remaining drug after release. FESEM imaging and PXRD spectra revealed the absence of NPX crystals, denoting complete drug release despite the presence of insoluble E100 matrix corroborating the observations of the UV−visible spectrophotometry-based release study (Figure S7, Section S5, Supporting Information).

NPX solubility estimated at equilibrium in SGF (pH 1.2) at 37 °C by UV−visible spectrophotometry was found to be 22.91 ± 1.19 μg/mL, close to the previously reported solubility of ~27 μg/mL.[92] The low solubility is because NPX is a weakly acidic (pK_a ~ 4.2) API.[29] Interestingly, the E100-NPX microparticles showed ~60−80% faster release compared to neat NPX microparticles in the first 15 min of release at pH 1.2 (Figure 5b). Complete dissolution for all E100-NPX microparticles was achieved within 8 h. The improvement in drug release from E100-NPX microparticles at pH 1.2 could be due to a combination of factors. First, E100 is soluble at pH 1.2 due to the protonation of tertiary amine groups promoting matrix dissolution. Second, as discussed in Section 3.4, incorporation of E100 increases the internal porosity and reduces the primary particle sizes, resulting in an increased influx of release media and subsequent faster drug solubilization. The initial release profiles for all the microparticles determined for the first 20 min of the release in pH 7.4 and 4 h of release in pH 1.2 followed first-order release kinetics (Figure 5a,b, insets) where the release rate is dependent on the undissolved drug mass. The release profiles of E100-NPX microparticles were further compared with neat NPX using FDA recommended difference ($f1$) and similarity ($f2$) factors (see Section S5, Supporting Information for details). The current in vitro setup at sink conditions enabled us to independently understand the potential impact of E100 excipient on drug release tunability of NPX and matrix dissolution of co-processed microparticles via modifications at the sub-particle level and difference in solubility of E100 at acidic and neutral pH values. Notably, when subjected to non-sink conditions (lower volume of pH 1.2, at room temperature), E100-NPX 0.25 microparticles still showed a faster release compared to that of neat NPX microparticles (see Section S5, Supporting Information for details). With these findings, a two-stage dissolution study with bio-relevant release volumes and time scales can be planned in future work.

3.5.3. Powder Rheology. Powder flowability is a major concern in pharmaceutical manufacturing because for a poorly flowing powder, it would be difficult to have a consistent powder dispensation, which in turn would affect the content uniformity of the tablet. Compared to the unprocessed, raw NPX (as-received from Sigma), neat NPX and E100-NPX 0.25 microparticles flowed much better when rotated in a glass vial (see Video S1, Supporting Information). Flow behavior across the three powder samples was further investigated using powder flow rheometry to acquire incipient failure or yield points as a

function of applied normal stress with pre-consolidation stress of 3 kPa. Data points were fitted to a linear equation followed by greater and smaller Mohr's circle fitting to obtain several flowability parameters including powder cohesion, unconfined yield stress, major principal stress, and flow factor. Figure 6
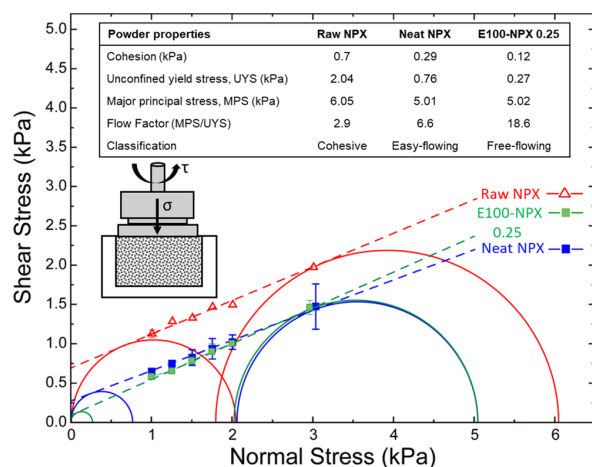

Figure 6. Incipient shear stress of powder flow as a function of the applied normal stress for unprocessed raw NPX (red color) and microfluidics-generated neat NPX (blue color) and E100-NPX 0.25 (green color) microparticles. Error bars correspond to standard deviations for triplicates for each group. The inset schematic shows the 1 mL shear cell test setup, and the inset table summarizes the powder flow metrics.

depicts the plot for the incipient shear stress of powder flow as a function of the applied normal stress for each of the three powder samples, and the inset table summarizes the flowability metrics. Raw NPX with a cohesion value of 0.7 kPa and a flow factor of 2.9 was the most cohesive and least flowable. Comparatively, microfluidics-generated neat NPX particles had a reduction in the cohesion value (0.29 kPa), and a significant increase in the flow factor to 6.6, putting them in the "easy-flowing" category.[93] With excipient addition, co-processed E100-NPX 0.25 microparticles were the least cohesive (cohesion value, 0.12 kPa) and were classified as "free-flowing" powders with the highest flow factor of 18.6.

With the same polymorphic forms of NPX in all the three powder samples, the significant differences in their powder flow behavior were attributed to the differences in their morphology, size, and composition. As shown in Figure 3, raw NPX particles have plate-like morphology, smallest particle size, and highest PDI encouraging higher particle–particle contact and interlocking that subsequently leads to cohesiveness and poor flowability. In comparison, the interparticle contact area is reduced for the particles produced via droplet microfluidics due to their spherical shape and narrow size distribution which gets translated into their lower cohesion values and better flowability. Between the two microfluidics-generated particles, E100-NPX 0.25 microparticles are less cohesive and more flowable which could be due to the possibly weakened interparticle interaction strength in the presence of E100 in microparticles, as also discussed previously by our group.[14] These structural and compositional differences lead to a substantial improvement in the flowability of E100-NPX microparticles. Further detailed studies on the compaction and tabletability of these co-

processed microparticles are the subjects of ongoing investigations.

4. CONCLUSIONS

This work presents an expanded use of Eudragit E100 (a cationic, pH-dependent excipient) to co-process a hydrophobic API into compact microparticles having a tunable solid-state and controlled particle attributes across multiple length scales. While E100 is cationic and soluble at low pH values, the model API NPX is anionic and shows poor solubility at low pH values. Co-processing of E100 with NPX is performed via droplet microfluidics that generates spherical and monodisperse microparticles with homogeneous spatial drug distribution. The solid-state outcome can be rationally tuned from amorphous at high E100 concentrations to crystalline at lower E100 concentrations. The detailed characterization of the crystalline E100-NPX microparticles reveals reduction in size of primary particles and enhancement of inner porosity due to E100. Owing to these E100-mediated structural changes and the solubility of E100 at lower pH values, the co-processed E100-NPX microparticles show faster drug release in acidic media despite the crystalline state of the API, thereby overcoming the poor NPX solubility at low pH. The morphological and compositional modifications make E100-NPX microparticles the least cohesive and with the highest flow factor elucidating their improved flowability compared to both raw NPX and neat NPX microparticles. To conclude, with rational particle engineering using droplet microfluidics, E100 was shown to improve the physical properties of the API without being used at a high concentration. We envision that our findings will provoke further studies to explore the application of E100, and other Eudragit polymers, for co-processing API into crystalline forms for use in oral solid dosage forms.

■ ASSOCIATED CONTENT

ⓢ Supporting Information

The Supporting Information is available free of charge at https://pubs.acs.org/doi/10.1021/acs.molpharmaceut.2c00714.

> Details on residual solvent analysis using TGA and NMR, Gordon–Taylor equation and plot for drug–excipient miscibility, bright-field microscopy images for particles used for size distribution analysis, confocal Raman mapping for spatial drug distribution, size and size distribution plot of primary particle size characterization, BET plot for porosity analysis, details on release kinetics and similarity/difference factors for release studies at pH 1.2 and 7.4, post-release characterization data for E100-NPX microparticles after release in pH 7.4, and release profiles for neat NPX and E100-NPX 0.25 microparticles under non-sink conditions at pH 1.2 (PDF)

> Flow videos of powder samples in glass vials (MP4)

■ AUTHOR INFORMATION

Corresponding Authors

Patrick S. Doyle − *Critical Analytics for Manufacturing Personalized-Medicine, Singapore-MIT Alliance for Research and Technology, Singapore 138602, Singapore; Department of Chemical Engineering, Massachusetts Institute of Technology, Cambridge, Massachusetts 02139, United States; Harvard Medical School Initiative for RNA Medicine, Boston,*

Massachusetts 02215, United States; ● orcid.org/0000-0003-2147-9172; Email: pdoyle@mit.edu

Saif A. Khan − *Department of Chemical and Biomolecular Engineering, National University of Singapore, Singapore 117576, Singapore;* ● orcid.org/0000-0002-8990-8802; Email: saifkhan@nus.edu.sg

Authors

Swati Shikha − *Critical Analytics for Manufacturing Personalized-Medicine, Singapore-MIT Alliance for Research and Technology, Singapore 138602, Singapore*

Yi Wei Lee − *Department of Chemical and Biomolecular Engineering, National University of Singapore, Singapore 117576, Singapore; NUS Graduate School for Integrative Sciences & Engineering, National University of Singapore, Singapore 119077, Singapore*

Complete contact information is available at:
https://pubs.acs.org/10.1021/acs.molpharmaceut.2c00714

■ REFERENCES

(1) Li, Z.; Lin, X.; Shen, L.; Hong, Y.; Feng, Y. Composite particles based on particle engineering for direct compaction. *Int. J. Pharm.* **2017**, *519*, 272−286.

(2) Li, Z.; Zhao, L.; Lin, X.; Shen, L.; Feng, Y. Direct compaction: An update of materials, trouble-shooting, and application. *Int. J. Pharm.* **2017**, *529*, 543−556.

(3) Chattoraj, S.; Sun, C. C. Crystal and particle engineering strategies for improving powder compression and flow properties to enable continuous tablet manufacturing by direct compression. *J. Pharm. Sci.* **2018**, *107*, 968−974.

(4) Chen, H.; Guo, Y.; Wang, C.; Dun, J.; Sun, C. C. Spherical cocrystallization—an enabling technology for the development of high dose direct compression tablets of poorly soluble drugs. *Cryst. Growth Des.* **2019**, *19*, 2503−2510.

(5) Huang, Z.; Scicolone, J. V.; Han, X.; Davé, R. N. Improved blend and tablet properties of fine pharmaceutical powders via dry particle coating. *Int. J. Pharm.* **2015**, *478*, 447−455.

(6) Kunnath, K.; Huang, Z.; Chen, L.; Zheng, K.; Davé, R. Improved properties of fine active pharmaceutical ingredient powder blends and tablets at high drug loading via dry particle coating. *Int. J. Pharm.* **2018**, *543*, 288−299.

(7) Chen, L.; He, Z.; Kunnath, K. T.; Fan, S.; Wei, Y.; Ding, X.; Zheng, K.; Davé, R. N. Surface engineered excipients: III. Facilitating direct compaction tableting of binary blends containing fine cohesive poorly-compactable APIs. *Int. J. Pharm.* **2019**, *557*, 354−365.

(8) Babu, N. J.; Nangia, A. Solubility advantage of amorphous drugs and pharmaceutical cocrystals. *Cryst. Growth Des.* **2011**, *11*, 2662−2679.

(9) Gupta, D.; Bhatia, D.; Dave, V.; Sutariya, V.; Varghese Gupta, S. Salts of therapeutic agents: chemical, physicochemical, and biological considerations. *Molecules* **2018**, *23*, 1719.

(10) Savjani, K. T.; Gajjar, A. K.; Savjani, J. K. Drug solubility: importance and enhancement techniques. *ISRN Pharm.* **2012**, *2012*, 195727.

(11) Kawashima, Y.; Cui, F.; Takeuchi, H.; Niwa, T.; Hino, T.; Kiuchi, K. Improvements in flowability and compressibility of pharmaceutical crystals for direct tabletting by spherical crystallization with a two-solvent system. *Powder Technol.* **1994**, *78*, 151−157.

(12) Kawashima, Y.; Imai, M.; Takeuchi, H.; Yamamoto, H.; Kamiya, K.; Hino, T. Improved flowability and compactibility of spherically agglomerated crystals of ascorbic acid for direct tableting designed by spherical crystallization process. *Powder Technol.* **2003**, *130*, 283−289.

(13) Nelson, A. Z.; Xie, J.; Khan, S. A.; Doyle, P. S. Continuous Embedded Droplet Printing in Yield-Stress Fluids for Pharmaceutical Drug Particle Synthesis. *Adv. Mater. Technol.* **2021**, *6*, 2001245.

(14) Ng, D. Z.; Nelson, A. Z.; Ward, G.; Lai, D.; Doyle, P. S.; Khan, S. A. Control of Drug-Excipient Particle Attributes with Droplet Microfluidic-based Extractive Solidification Enables Improved Powder Rheology. *Pharm. Res.* **2022**, *39*, 411−421.

(15) Yeap, E. W.; Acevedo, A. J.; Khan, S. A. Microfluidic extractive crystallization for spherical drug/drug-excipient microparticle production. *Org. Process Res. Dev.* **2019**, *23*, 375−381.

(16) Liu, L. X.; Marziano, I.; Bentham, A.; Litster, J. D.; White, E.; Howes, T. Effect of particle properties on the flowability of ibuprofen powders. *Int. J. Pharm.* **2008**, *362*, 109−117.

(17) Hancock, B. C.; Parks, M. What is the true solubility advantage for amorphous pharmaceuticals? *Pharm. Res.* **2000**, *17*, 397−404.

(18) Joiris, E.; Martino, P. D.; Berneron, C.; Guyot-Hermann, A.-M.; Guyot, J.-C. Compression behavior of orthorhombic paracetamol. *Pharm. Res.* **1998**, *15*, 1122−1130.

(19) Szabó, E.; Démuth, B.; Galata, D. L.; Vass, P.; Hirsch, E.; Csontos, I.; Marosi, G.; Nagy, Z. K. Continuous formulation approaches of amorphous solid dispersions: significance of powder flow properties and feeding performance. *Pharmaceutics* **2019**, *11*, 654.

(20) Aitipamula, S.; Banerjee, R.; Bansal, A. K.; Biradha, K.; Cheney, M. L.; Choudhury, A. R.; Desiraju, G. R.; Dikundwar, A. G.; Dubey, R.; Duggirala, N.; Ghogale, P. P.; Ghosh, S.; Goswami, P. K.; Goud, N. R.; Jetti, R. R. K. R.; Karpinski, P.; Kaushik, P.; Kumar, D.; Kumar, V.; Moulton, B.; Mukherjee, A.; Mukherjee, G.; Myerson, A. S.; Puri, V.; Ramanan, A.; Rajamannar, T.; Reddy, C. M.; Rodriguez-Hornedo, N.; Rogers, R. D.; Row, T. N. G.; Sanphui, P.; Shan, N.; Shete, G.; Singh, A.; Sun, C. C.; Swift, J. A.; Thaimattam, R.; Thakur, T. S.; Kumar Thaper, R.; Thomas, S. P.; Tothadi, S.; Vangala, V. R.; Variankaval, N.; Vishweshwar, P.; Weyna, D. R.; Zaworotko, M. J. Polymorphs, Salts, and Cocrystals: What's in a Name? *Cryst. Growth Des.* **2012**, *12*, 2147−2152.

(21) Aguiar, A. J.; Krc, J., Jr.; Kinkel, A. W.; Samyn, J. C. Effect of polymorphism on the absorption of chloramphenicol from chloramphenicol palmitate. *J. Pharm. Sci.* **1967**, *56*, 847−853.

(22) Erdemir, D.; Daftary, V.; Lindrud, M.; Buckley, D.; Lane, G.; Malsbury, A.; Tao, J.; Kopp, N.; Hsieh, D. S.; Nikitczuk, W.; Engstrom, J. D. Design and scale-up of a co-processing technology to improve powder properties of drug substances. *Org. Process Res. Dev.* **2019**, *23*, 2685−2698.

(23) Erdemir, D.; Rosenbaum, T.; Chang, S.-Y.; Wong, B.; Kientzler, D.; Wang, S.; Desai, D.; Kiang, S. Novel co-processing methodology to enable direct compression of a poorly compressible, highly water-soluble active pharmaceutical ingredient for controlled release. *Org. Process Res. Dev.* **2018**, *22*, 1383−1392.

(24) Maghsoodi, M.; Kiafar, F. Co-precipitation with PVP and agar to improve physicomechanical properties of ibuprofen. *Iran. J. Basic Med. Sci.* **2013**, *16*, 602.

(25) Schenck, L.; Erdemir, D.; Saunders Gorka, L.; Merritt, J. M.; Marziano, I.; Ho, R.; Lee, M.; Bullard, J.; Boukerche, M.; Ferguson, S.;

Florence, A. J.; Khan, S. A.; Sun, C. C. Recent advances in co-processed APIs and proposals for enabling commercialization of these transformative technologies. *Mol. Pharmaceutics* 2020, 17, 2232−2244.

(26) Ting, J. M.; Porter, W. W., III; Mecca, J. M.; Bates, F. S.; Reineke, T. M. Advances in polymer design for enhancing oral drug solubility and delivery. *Bioconjugate Chem.* 2018, 29, 939−952.

(27) Yeap, E. W.; Ng, D. Z.; Prhashanna, A.; Somasundar, A.; Acevedo, A. J.; Xu, Q.; Salahioglu, F.; Garland, M. V.; Khan, S. A. Bottom-up structural design of crystalline drug-excipient composite microparticles via microfluidic droplet-based processing. *Cryst. Growth Des.* 2017, 17, 3030−3039.

(28) Ho, L. Y.; Xiang, Z. S.; Gopal, R.; Khan, S. A. Microfluidics-enabled particle engineering of monodisperse solid lipid microparticles with uniform drug loading and diverse solid-state outcomes. *Int. J. Pharm.* 2021, 596, 120230.

(29) Doreth, M.; Löbmann, K.; Grohganz, H.; Holm, R.; Lopez de Diego, H.; Priemel, T.; Priemel, P. A. Glass solution formation in water - In situ amorphization of naproxen and ibuprofen with Eudragit E PO. *J. Drug Delivery Sci. Technol.* 2016, 34, 32−40.

(30) Ofridam, F.; Tarhini, M.; Lebaz, N.; Gagnière, E.; Mangin, D.; Elaissari, A. pH -sensitive polymers: Classification and some fine potential applications. *Polym. Adv. Technol.* 2021, 32, 1455−1484.

(31) Amelian, A.; Winnicka, K. Polymers in pharmaceutical taste masking applications. *Polimery* 2017, 62, 419−427.

(32) Thakral, S.; Thakral, N. K.; Majumdar, D. K. Eudragit: a technology evaluation. *Expert Opin. Drug Delivery* 2013, 10, 131−149.

(33) Nikam, V. K.; Kotade, K.; Gaware, V.; Dolas, R.; Dhamak, K.; Somwanshi, S.; Khadse, A. N.; Kashid, V. A. Eudragit a versatile polymer: a review. *Pharmacologyonline* 2011, 1, 152−164.

(34) Hamzehloo, M.; Karimi, J.; Eghbali, N.; Mirzakhani, M.; Aghapoor, K.; Darabi, H. R. A new blend of polymeric encapsulation of azithromycin by spray-drying with a pH responsive in drug release. *Drying Technol.* 2017, 35, 1688−1695.

(35) Patil, S. S.; Roy, K.; Choudhary, B.; Mahadik, K. R. Fabrication of novel GMO/Eudragit E100 nanostructures for enhancing oral bioavailability of carvedilol. *Drug Dev. Ind. Pharm.* 2016, 42, 1300−1307.

(36) Prasad, D.; Chauhan, H.; Atef, E. Amorphous stabilization and dissolution enhancement of amorphous ternary solid dispersions: combination of polymers showing drug−polymer interaction for synergistic effects. *J. Pharm. Sci.* 2014, 103, 3511−3523.

(37) Shah, P.; Mashru, R.; Rane, Y.; Badhan, A. Design and optimization of artemether microparticles for bitter taste masking. *Acta Pharm.* 2008, 58, 379.

(38) Kumar, B. P.; Archana, G.; Swarupa, Y.; Devi, K. J. Formulation and evaluation of nizatidine fast dissolving tablets. *World J. Pharm. Res.* 2015, 4, 1358−1372.

(39) Fine-Shamir, N.; Dahan, A. Methacrylate-copolymer Eudragit EPO as a solubility-enabling excipient for anionic drugs: investigation of drug solubility, intestinal permeability, and their interplay. *Mol. Pharm.* 2019, 16, 2884−2891.

(40) Han, C.-S.; Kim, S.; Oh, D.-W.; Yoon, J. Y.; Park, E.-S.; Rhee, Y.-S.; Kim, J.-Y.; Shin, D. H.; Kim, D.-W.; Park, C.-W. Preparation, characterization, and stability evaluation of taste-masking Lacosamide microparticles. *Materials* 2019, 12, 1000.

(41) Chiappetta, D. A.; Carcaboso, Á. M.; Bregni, C.; Rubio, M.; Bramuglia, G.; Sosnik, A. Indinavir-loaded pH-sensitive microparticles for taste masking: toward extemporaneous pediatric anti-HIV/AIDS liquid formulations with improved patient compliance. *AAPS PharmSciTech* 2009, 10, 1−6.

(42) Montaña, J. A.; Perez, L. D.; Baena, Y. A pH-responsive drug delivery matrix from an interpolyelectrolyte complex: preparation and pharmacotechnical properties. *Braz. J. Pharm. Sci.* 2018, 54, 1.

(43) Bukhovets, A. V.; Fotaki, N.; Khutoryanskiy, V. V.; Moustafine, R. I. Interpolymer Complexes of Eudragit Copolymers as Novel Carriers for Colon-Specific Drug Delivery. *polymers* 2020, 12, 1459.

(44) Obeidat, W. M.; Nokhodchi, A.; Alkhatib, H. Evaluation of Matrix Tablets Based on EudragitE100/Carbopol971P Combinations for Controlled Release and Improved Compaction Properties of Water

Soluble Model Drug Paracetamol. *AAPS PharmSciTech* 2015, 16, 1169−1179.

(45) Rohilla, S.; Bhatt, D. C.; Ahalwat, S. Effect processing variables on the characteristics of itraconazole hollow microspheres. *Int. J. Appl. Pharm.* 2019, 11, 108−115.

(46) Farooq, U.; Khan, S.; Nawaz, S.; Ranjha, N. M.; Haider, M. S.; Khan, M. M.; Dar, E.; Nawaz, A. Enhanced gastric retention and drug release via development of novel floating microspheres based on Eudragit E100 and polycaprolactone: synthesis and in vitro evaluation. *Des. Monomers Polym.* 2017, 20, 419−433.

(47) Tian, Y.; Jacobs, E.; Jones, D. S.; McCoy, C. P.; Wu, H.; Andrews, G. P. The design and development of high drug loading amorphous solid dispersion for hot-melt extrusion platform. *Int. J. Pharm.* 2020, 586, 119545.

(48) Lubach, J. W.; Hau, J. Solid-state NMR investigation of drug-excipient interactions and phase behavior in indomethacin-Eudragit E amorphous solid dispersions. *Pharm. Res.* 2018, 35, 65.

(49) Six, K.; Leuner, C.; Dressman, J.; Verreck, G.; Peeters, J.; Blaton, N.; Augustijns, P.; Kinget, R.; Van den Mooterguy.vandenmooter@ farm.kuleuven.ac.be, G. Thermal properties of hot-stage extrudates of itraconazole and eudragit E100. Phase separation and polymorphism. *J. Therm. Anal. Calorim.* 2002, 68, 591−601.

(50) Janssens, S.; De Zeure, A.; Paudel, A.; Van Humbeeck, J.; Rombaut, P.; Van den Mooter, G. Influence of preparation methods on solid state supersaturation of amorphous solid dispersions: a case study with itraconazole and eudragit e100. *Pharm. Res.* 2010, 27, 775−785.

(51) Frank, D. S.; Prasad, P.; Iuzzolino, L.; Schenck, L. Dissolution behavior of weakly basic pharmaceuticals from amorphous dispersions stabilized by a poly(dimethylaminoethyl Methacrylate) copolymer. *Mol. Pharmaceutics* 2022, 19, 3304.

(52) Yu, L. Amorphous pharmaceutical solids: preparation, characterization and stabilization. *Adv. Drug Delivery Rev.* 2001, 48, 27−42.

(53) Blagden, N.; de Matas, M.; Gavan, P. T.; York, P. Crystal engineering of active pharmaceutical ingredients to improve solubility and dissolution rates. *Adv. Drug Delivery Rev.* 2007, 59, 617−630.

(54) Kobayashi, Y.; Ito, S.; Itai, S.; Yamamoto, K. Physicochemical properties and bioavailability of carbamazepine polymorphs and dihydrate. *Int. J. Pharm.* 2000, 193, 137−146.

(55) Wang, Y.; Zhang, N.; Hou, B.; Yin, Q.; Gong, J.; Tang, W. Effect of crystal growth kinetics on the formation of liquid inclusions in tetramethylpyrazine crystals. *CrystEngComm* 2020, 22, 1991−2001.

(56) Orehek, J.; Teslić, D.; Likozar, B. Continuous crystallization processes in pharmaceutical manufacturing: A review. *Org. Process Res. Dev.* 2020, 25, 16−42.

(57) Hatcher, L. E.; Burgess, A. J.; Payne, P.; Wilson, C. C. From structure to crystallisation and pharmaceutical manufacturing: the CSD in CMAC workflows. *CrystEngComm* 2020, 22, 7475−7489.

(58) Hadjittofis, E.; Isbell, M. A.; Karde, V.; Varghese, S.; Ghoroi, C.; Heng, J. Y. Influences of crystal anisotropy in pharmaceutical process development. *Pharm. Res.* 2018, 35, 100.

(59) Chikukwa, M. T.; Walker, R. B.; Khamanga, S. M. Formulation and characterisation of a combination captopril and hydrochlorothiazide microparticulate dosage form. *Pharmaceutics* 2020, 12, 712.

(60) Wegiel, L. A.; Mauer, L. J.; Edgar, K. J.; Taylor, L. S. Crystallization of amorphous solid dispersions of resveratrol during preparation and storage—Impact of different polymers. *J. Pharm. Sci.* 2013, 102, 171−184.

(61) Bedor, D. C. G.; Bedor, N. C. T. C.; Neto, J. G. P.; José de Alencar Danda, L.; de Oliveira, F. M.; de Oliveira, G. H. O.; Soares Sobrinho, J. L.; Beyssac, E.; Castro, W. V. d.; Santana, D. P. d. Characterization, in vitro dissolution, and pharmacokinetics of different batches of efavirenz raw materials. *Drug Dev. Ind. Pharm.* 2021, 47, 725−734.

(62) Kim, J. M.; Kim, D. H.; Park, H. J.; Ma, H. W.; Park, I. S.; Son, M.; Ro, S. Y.; Hong, S.; Han, H. K.; Lim, S. J. Nanocomposites-based targeted oral drug delivery systems with infliximab in a murine colitis model. *J. Nanobiotechnol.* 2020, 18, 133.

(63) Sah, S. K.; Joshi, D.; Pathak, S.; Regmi, S.; Regmi, B.; Man, P.; Marasini, N. Effect of Ethanol and pH on the In Vitro adsorption of

Diazepam onto activated charcoal from simulated gastric fluid and simulated intestinal fluid. *Indian J. Pharm. Sci.* **2016**, *78*, 624−630.

(64) Ueda, H.; Wakabayashi, S.; Kikuchi, J.; Ida, Y.; Kadota, K.; Tozuka, Y. Anomalous role change of tertiary amino and ester groups as hydrogen acceptors in eudragit E based solid dispersion depending on the concentration of naproxen. *Mol. Pharmaceutics* **2015**, *12*, 1050−1061.

(65) Linares, V.; Yarce, C. J.; Echeverri, J. D.; Galeano, E.; Salamanca, C. H. Relationship between Degree of Polymeric Ionisation and Hydrolytic Degradation of Eudragit E Polymers under Extreme Acid Conditions. *Polymers* **2019**, *11*, 1010.

(66) Song, J.-S.; Sohn, Y.-T. Crystal forms of naproxen. *Arch. Pharmacal Res.* **2011**, *34*, 87−90.

(67) Abraham, N. S.; El−Serag, H. B.; Johnson, M. L.; Hartman, C.; Richardson, P.; Ray, W. A.; Smalley, W. National adherence to evidence-based guidelines for the prescription of nonsteroidal anti-inflammatory drugs. *Gastroenterology* **2005**, *129*, 1171−1178.

(68) International Council For Harmonisation Of Technical Requirements For Pharmaceuticals for Human Use. IMPURITIES: GUIDELINE FOR RESIDUAL SOLVENTS Q3C(R8), 2021. https://database.ich.org/sites/default/files/ICH_Q3C-R8_Guideline_Step4_2021_0422_1.pdf (accessed May 23, 2022).

(69) Baird, J. A.; Van Eerdenbrugh, B.; Taylor, L. S. A classification system to assess the crystallization tendency of organic molecules from undercooled melts. *J. Pharm. Sci.* **2010**, *99*, 3787−3806.

(70) Kawakami, K. Crystallization tendency of pharmaceutical glasses: relevance to compound properties, impact of formulation process, and implications for design of amorphous solid dispersions. *Pharmaceutics* **2019**, *11*, 202.

(71) Yeap, E. W.; Ng, D. Z.; Lai, D.; Ertl, D. J.; Sharpe, S.; Khan, S. A. Continuous flow droplet-based crystallization platform for producing spherical drug microparticles. *Org. Process Res. Dev.* **2018**, *23*, 93−101.

(72) Gordon, M.; Taylor, J. S. Ideal copolymers and the second-order transitions of synthetic rubbers. I. Non-crystalline copolymers. *J. Appl. Chem.* **1952**, *2*, 493−500.

(73) Ricarte, R. G.; Van Zee, N. J.; Li, Z.; Johnson, L. M.; Lodge, T. P.; Hillmyer, M. A. Recent advances in understanding the micro-and nanoscale phenomena of amorphous solid dispersions. *Mol. Pharmaceutics* **2019**, *16*, 4089−4103.

(74) Medarević, D.; Djuriš, J.; Barmpalexis, P.; Kachrimanis, K.; Ibrić, S. Analytical and computational methods for the estimation of drug-polymer solubility and miscibility in solid dispersions development. *Pharmaceutics* **2019**, *11*, 372.

(75) Qian, F.; Huang, J.; Zhu, Q.; Haddadin, R.; Gawel, J.; Garmise, R.; Hussain, M. Is a distinctive single Tg a reliable indicator for the homogeneity of amorphous solid dispersion? *Int. J. Pharm.* **2010**, *395*, 232−235.

(76) Hurley, D.; Davis, M.; Walker, G. M.; Lyons, J. G.; Higginbotham, C. L. The effect of cooling on the degree of crystallinity, solid-state properties, and dissolution rate of multi-component hot-melt extruded solid dispersions. *Pharmaceutics* **2020**, *12*, 212.

(77) Higashi, K.; Ueda, K.; Moribe, K. Intermolecular interactions between drugs and aminoalkyl methacrylate copolymer in solution to enhance the concentration of poorly water-soluble drugs. *Chem. Pharm. Bull.* **2019**, *67*, 906−914.

(78) Quinteros, D. A.; Rigo, V. R.; Kairuz, A. F. J.; Olivera, M. E.; Manzo, R. H.; Allemandi, D. A. Interaction between a cationic polymethacrylate (Eudragit E100) and anionic drugs. *Eur. J. Pharm. Sci.* **2008**, *33*, 72−79.

(79) Ramírez-Rigo, M. V.; Olivera, M. E.; Rubio, M.; Manzo, R. H. Enhanced intestinal permeability and oral bioavailability of enalapril maleate upon complexation with the cationic polymethacrylate Eudragit E100. *Eur. J. Pharm. Sci.* **2014**, *55*, 1−11.

(80) Wegiel, L. A.; Mauer, L. J.; Edgar, K. J.; Taylor, L. S. Mid-infrared spectroscopy as a polymer selection tool for formulating amorphous solid dispersions. *J. Pharm. Pharmacol.* **2014**, *66*, 244−255.

(81) Pitt, K.; Peña, R.; Tew, J. D.; Pal, K.; Smith, R.; Nagy, Z. K.; Litster, J. D. Particle design via spherical agglomeration: A critical review of controlling parameters, rate processes and modelling. *Powder Technol.* **2018**, *326*, 327−343.

(82) de Veij, M.; Vandenabeele, P.; De Beer, T.; Remon, J. P.; Moens, L. Reference database of Raman spectra of pharmaceutical excipients. *J. Raman Spectrosc.* **2009**, *40*, 297−307.

(83) Zhang, J.; Ying, Y.; Pielecha-Safira, B.; Bilgili, E.; Ramachandran, R.; Romañach, R.; Davé, R. N.; Iqbal, Z. Raman spectroscopy for in-line and off-line quantification of poorly soluble drugs in strip films. *Int. J. Pharm.* **2014**, *475*, 428−437.

(84) Verma, V.; Peddapatla, R. V.; Crowley, C. M.; Crean, A. M.; Davern, P.; Hudson, S.; Hodnett, B. K. Experimental study on the influence of excipients on the heterogeneous crystallization and dissolution properties of an active pharmaceutical ingredient. *Cryst. Growth Des.* **2018**, *18*, 338−350.

(85) Huang, X.; Brazel, C. S. On the importance and mechanisms of burst release in matrix-controlled drug delivery systems. *J. Controlled Release* **2001**, *73*, 121−136.

(86) Reza, M. S.; Quadir, M. A.; Haider, S. S. Comparative evaluation of plastic, hydrophobic and hydrophilic polymers as matrices for controlled-release drug delivery. *J. Pharm. Pharm. Sci.* **2003**, *6*, 282−291.

(87) Young, P. M.; Nguyen, K.; Jones, A. S.; Traini, D. Microstructural analysis of porous composite materials: dynamic imaging of drug dissolution and diffusion through porous matrices. *AAPS J.* **2008**, *10*, 560−564.

(88) Ahuja, G.; Pathak, K. Porous carriers for controlled/modulated drug delivery. *Indian J. Pharm. Sci.* **2009**, *71*, 599.

(89) Divya, S.; Ganesh, G. Characterization of Powder Flowability Using FT4−Powder Rheometer. *J. Pharm. Sci. Res.* **2019**, *11*, 25−29.

(90) Jafari, E. Preparation, characterization and dissolution of solid dispersion of diclofenac sodium using Eudragit E-100. *J. Appl. Pharm. Sci.* **2013**, *3*, 167.

(91) Kumar, L.; Suhas, B.; Pai, G.; Verma, R. Determination of saturated solubility of naproxen using UV visible spectrophotometer. *Res. J. Pharm. Technol.* **2015**, *8*, 825−828.

(92) Lam, M.; Ghafourian, T.; Nokhodchi, A. Liqui-pellet: the emerging next-generation oral dosage form which stems from liquisolid concept in combination with pelletization technology. *AAPS PharmSciTech* **2019**, *20*, 231.

(93) Schulze, D. Flow properties of bulk solids. *Powders and Bulk Solids*; Springer, 2021; pp 57−100.

■ NOTE ADDED AFTER ASAP PUBLICATION

Originally published ASAP October 21, 2022; Section S1 of Supporting Information updated October 25, 2022.